AGU PUBLICATIONS

Geophysical Research Letters

RESEARCH LETTER
10.1002/2017GL074175

Key Points:
- Using a new detection scheme, a 69 yearlong catalog of atmospheric rivers land-falling upon western North America is created and validated
- AR landfalls show a marked seasonal progression from the Gulf of Alaska in the early fall to northern California in early winter
- The seasonal intensity of AR landfalls varies from year to year and from decade to decade in relation to Pacific SST variability

Supporting Information:
- Supporting Information S1

Correspondence to:
A. Gershunov,
sasha@ucsd.edu

Citation:
Gershunov, A., T. Shulgina, F. M. Ralph, D. A. Lavers, and J. J. Rutz (2017), Assessing the climate-scale variability of atmospheric rivers affecting western North America, *Geophys. Res. Lett.*, *44*, 7900–7908, doi:10.1002/2017GL074175.

Received 22 MAY 2017
Accepted 23 JUN 2017
Published online 3 AUG 2017

Assessing the climate-scale variability of atmospheric rivers affecting western North America

Alexander Gershunov[1], Tamara Shulgina[1], F. Martin Ralph[1], David A. Lavers[2], and Jonathan J. Rutz[3]

[1]Center for Western Weather and Water Extremes (CW3E), Scripps Institution of Oceanography, University of California, San Diego, La Jolla, California, USA, [2]European Centre for Medium-Range Weather Forecasts (ECMWF), Reading, UK, [3]Science and Technology Infusion Division, National Weather Service, Western Region Headquarters, Salt Lake City, Utah, USA

Abstract A new method for automatic detection of atmospheric rivers (ARs) is developed and applied to an atmospheric reanalysis, yielding an extensive catalog of ARs land-falling along the west coast of North America during 1948–2017. This catalog provides a large array of variables that can be used to examine AR cases and their climate-scale variability in exceptional detail. The new record of AR activity, as presented, validated and examined here, provides a perspective on the seasonal cycle and the interannual-interdecadal variability of AR activity affecting the hydroclimate of western North America. Importantly, AR intensity does not exactly follow the climatological pattern of AR frequency. Strong links to hydroclimate are demonstrated using a high-resolution precipitation data set. We describe the seasonal progression of AR activity and diagnose linkages with climate variability expressed in Pacific sea surface temperatures, revealing links to Pacific decadal variability, recent regional anomalies, as well as a generally rising trend in land-falling AR activity. The latter trend is consistent with a long-term increase in vapor transport from the warming North Pacific onto the North American continent. The new catalog provides unprecedented opportunities to study the climate-scale behavior and predictability of ARs affecting western North America.

Plain Language Summary We have created a new seven-decade-long catalog of atmospheric river behavior land-falling upon the west coast of North America. The catalog has been validated against independent precipitation observations to ensure that the atmospheric rivers represented therein are associated with extreme orographic precipitation. Our results clearly delineate a prominent role for atmospheric rivers in California's hydroclimate. Atmospheric river variability has been particularly important in the recent California drought as well as its most recent lapse. We also detect a long-term increasing trend in water vapor transport impinging on the west coast of North America associated with atmospheric rivers and overall wintertime water vapor transport associated with climate warming. Our results, moreover, suggest that potential predictability of seasonal behavior of atmospheric rivers may hinge on sources of climatic variability somewhat different from that of total water vapor transport.

1. Introduction

Atmospheric rivers (ARs) concentrate and accomplish significant moisture transport from the tropical to high latitudes [*Zhu and Newell*, 1998]. These filamentary features of the low troposphere are statically stable and can produce copious amounts of precipitation as long as an external uplifting mechanism is available [*Ralph et al*., 2006, 2011]. Land-falling ARs, therefore, greatly impact hydrology along the west coasts of continents, particularly where substantial orography is present. Their impacts are felt across the midlatitudes and even as far as the polar regions, where they contribute to the ice sheet surface mass balance [*Gorodetskaya et al*., 2014]. The west coast of North America is an example of a region where hydroclimate swings to the beat of AR landfalls. In California's Mediterranean climate, where total annual precipitation is generated in a narrow seasonal window, the difference between wet and dry years is typically due to the occurrence or absence of a few big winter storms [*Dettinger et al*., 2011; *Dettinger*, 2015; *Ralph and Dettinger*, 2011], and hydroclimate and water resource management are particularly sensitive to AR activity.

Along the west coast of North America, atmospheric circulation and precipitation are known to respond to interannual and interdecadal modes of climate variability [e.g., *Gershunov and Barnett*, 1998] expressed in Pacific sea surface temperature (SST) anomalies, a fact that accounts for significant seasonal predictability of precipitation, heavy precipitation frequency in particular [*Gershunov and Cayan*, 2003]. ARs are strongly

linked to heavy precipitation over the orographically complex western United States [*Rutz et al*., 2014]. They represent an episodic dynamical mechanism responsible for much of the moisture transport in the midlatitudes. Assessing land-falling AR behavior on climate time scales should lead to improved understanding of hydroclimate variability, likely leading to improved seasonal predictability.

Quantifying and assessing interannual-interdecadal variability in AR activity is clearly important; however, adequate records for such work have not been available until recently. Traditionally, development of AR catalogs has relied on satellite retrievals of atmospheric moisture, was based on vertically integrated water vapor (IWV), and limited to the satellite era [*Neiman et al*., 2008]. We hereby refer to the SSM/I IWV-based *Neiman et al.* [2008] catalog as "RNW," according to the last names of the authors who proposed the approach [*Ralph et al*., 2004]. Recent versions of IWV-based AR catalogs were developed by automated detection schemes from satellite data by *Wick et al*. [2013] and from reanalysis products [*Jackson et al*., 2016] and used to assess and compare cold-season landfall frequencies along the North American West Coast between these different products during the satellite era.

An essential feature of ARs is that they *move* water vapor. Thus, vertically integrated horizontal vapor transport (IVT), being a product of wind and moisture, more fully reflects the water vapor flux essence of ARs and is likely more closely associated with extreme orographic precipitation than is IWV alone [*Swales et al*., 2016]. Automated AR detection methodologies based on IVT data from *reanalyses* are becoming available [e.g., *Lavers et al*., 2012; *Rutz et al*., 2014; *Payne and Magnusdottir*, 2014; *Guan and Waliser*, 2015; *Brands et al*., 2016; *Eiras-Barca et al*., 2016; *Mundhenk et al*., 2016]; however, each of these has their strengths and weaknesses having been developed for different applications, and the resulting catalogs are typically not validated against independent precipitation data, nor do they include all variables of interest, e.g., IVT, IWV, wind speed, and direction, over the impacted region. Importantly, the available catalogs start in 1979, with the notable exception of *Brands et al*. [2016], and are not long enough to resolve interdecadal variability, particularly the mid-1970s North Pacific climate shift [e.g., *Mantua et al*., 1997]. This prompts us to develop a new AR detection methodology (ARDT) based on both IVT and IWV measures to independently identify ARs in reanalysis products with relatively long records and demonstrate their association with heavy precipitation. We start with the National Center of Environmental Prediction-National Center for Atmospheric Research reanalysis (R1, *Kalnay et al.* [1996]), which covers 69+ years, yielding a record long enough to allow a comprehensive examination of climate-scale variability in AR activity along the west coast of North America.

Below, we report on our automated AR detection methodology (section 2 and supporting information section S1), apply it to R1, and, after validating the records thus obtained against (a) a shorter established satellite-based record (i.e., RNW), (b) independent precipitation observations, and (c) a longer and arguably more stable reanalysis product (supporting information section S2), we present the year-round climatology of monthly AR landfalls along with their IVT intensity, IWV content, and wind measures (section 3). We then examine climate-scale variability of AR activity along the North American West Coast (section 4) and conclude with implications, including those for potentially improving seasonal predictability (section 5).

2. AR Detection Methodology (ARDT) and Validation

Our AR detection methodology (ARDT) is described in detail in supporting information section S1. Although this method is technically unique, we do not claim methodological novelty as it shares many features with other available AR detection methods. The main benefits of our ARDT are as follows: it provides a long and validated (see supporting information section S2) record of AR activity at the North American West Coast with established links to orographic precipitation (see supporting information section S2b) and a broad array of variables we require for this and future analyses (see supporting information section S1). We refer to this Scripps Institution of Oceanography (SIO)-generated AR catalog as the *SIO-R1 catalog*.

We validated SIO-R1 in three ways: (1) by comparing it against the RNW catalog developed by *Neiman et al*. [2008] and recently updated through 2015, (2) by assessing the contribution of ARs from both the SIO-R1 and the RNW catalogs to observed precipitation resolved daily over the West on a 6 × 6 km grid [*Livneh et al*., 2013], and (3) by comparing presatellite and satellite era AR climatologies with those derived by application of our ARDT to the NOAA 20th Century Reanalysis [*Compo et al*., 2011]. Validation results are presented in supporting information section S2. In summary, there is significant agreement between SIO-R1 and RNW as far as the strongest ARs are concerned (Figure S1). However, compared to the IWV-based RNW, the

SIO-R1 contains more ARs in winter and fewer ARs in the less windy but more humid summer. Moreover, SIO-R1 is associated with more accumulated precipitation as well as with more intense precipitation events, yielding ARs that are clearly strongly associated with heavy orographic precipitation over the coastal ranges and to some extent over the inland topography of the mountainous West (Figure S2). What's more, SIO-R1, accounts best for heavy precipitation over the interior southwestern mountains and deserts (Figure S2), which is associated with ARs land-falling over Baja California [*Rutz and Steenburgh*, 2012; *Rivera et al*., 2014] that are missing from RNW. Additionally, we do not see any spurious discontinuities in the SIO-R1 data that may have been due to the introduction of satellite data in the 1970s (supporting information section S2c), justifying the use of SIO-R1 in studies of land-falling AR activity from a long-term climatological perspective.

3. AR Climatology

The climatology of AR landfalls at the North American West Coast during 1948–2015 is described next by showing average frequency, duration, and intensity of AR cases present in the SIO-R1 catalog by month and land-falling latitude (Figure 1). Wind vectors at coastal grid cells during AR landfalls were assessed at 850 hPa (Figure S7).

The climatological frequency of ARs by month and land-falling latitude is shown in Figure 1a. The core of AR activity migrates from the Gulf of Alaska and British Columbia in the late summer-fall to the Washington-Oregon-Northern California coast in winter. This seasonality in AR frequencies is in good agreement with that described by *Mundhenk et al.* [2016]. Regions of most frequent ARs, moreover, tend to receive the longest duration ARs, up to 2 days on climatological average (Figure 1b). Spring and summer are relative lulls in classic IVT/wind-driven AR activity, especially along coastal Baja California and California State, respectively (Figures 1a, 1b, and S7). Summer and early fall, however, represent the humid season in Baja and Southern California when very infrequent ARs can be quite long-lasting, moist, and windy (Figures 1b–1d and S7)—more moist in fact than is common or possible elsewhere and in other seasons. We have verified that of the 22 tropical storms (from the National Hurricane Center's records provided online: http://weather.unisys.com/hurricane/e_pacific/) that made landfall at subtropical latitudes in August–September (one occurred in July) during 1948–2015, all registered as AR landfalls. Although this explains only about 20% of AR landfalls registered below 30°N in August and September, we suspect that the majority of these were associated with tropical depressions and moisture plumes characteristic of decaying Eastern Pacific hurricanes and tropical storms.

AR intensity does not follow the same climatological pattern as does AR frequency. The intensity of ARs was estimated in terms of their IVT and IWV (Figures 1c and 1d) at coastal coordinates where ARs made landfall. Monthly total IVT and IWV associated with AR landfalls (not shown) reflect AR landfall frequency (Figure 1a). The IVT magnitude averaged over 6 hourly intervals during AR landfalls (Figure 1c) generally displays a similar seasonality as landfall frequency, being strongest in fall and winter at high latitudes. However, the absolute peak in AR magnitude does not necessarily follow AR frequency in its southward migration from late summer to winter. In the midlatitudes, unlike frequency, which peaks in British Columbia in October, AR intensity peaks in far Northern California in December. In this region, practically all of the floods along the Russian River are known to be associated with AR landfalls [*Ralph et al*., 2006]. The tropical and subtropical latitudes, however, experience the strongest IVT even though AR conditions register very infrequently (Figure 1a). Particularly in September (Figures 1c and 1d) when average IVT magnitude reaches up to 440 kg/m/s, IWV reaches about 40 mm, and wind rises to 15 m/s (Figure S7) on average during conditions detected as AR landfalls. Intensity together with the seasonal timing of landfalls at low latitudes and rudimentary verification using tropical storm records described above strongly suggest advection of tropical moisture plumes associated with eastern Pacific tropical storms.

The AR-related IVT at the high midlatitudes (British Columbia, Washington, and Oregon) tends to reach its maximum intensity during October–December (~450 kg/m/s on average, Figure 1d) accompanied by strong WSW winds (Figure S7) up to 18 m/s on average at 850 hPa. Note that especially in this early part of the cold season, AR-related precipitation can penetrate inland reaching the Northern Rockies (Figure S8), e.g., through the Columbia River Valley [*Rutz et al*., 2014] (also Figure 2c below). Wind speed and direction (Figure S7) during AR landfalls follow the fall-winter migration of AR activity from high to middle latitudes (Figure 1). At low latitudes (Baja California, Mexico), winds are strong from August to February but exhibit a seasonal

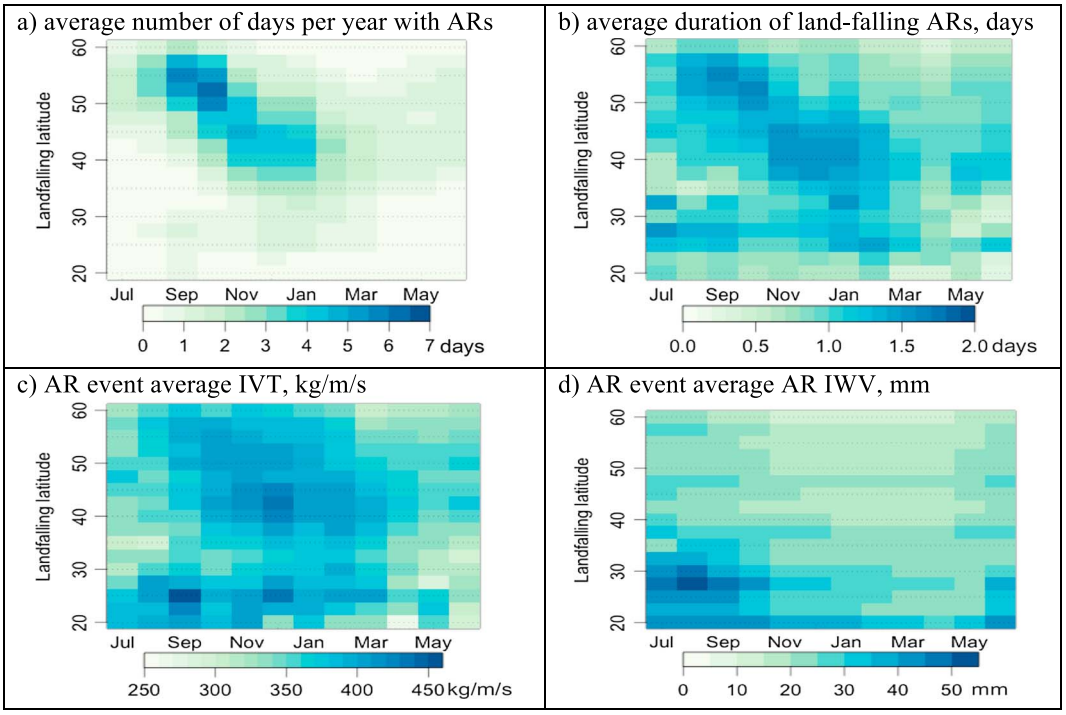

Figure 1. Monthly climatology of 6 hourly AR records expressed as (a) land-falling day counts, (b) average local land-falling duration, (c) average IVT per AR land-falling event, (d) and AR event average IWV, all presented by month and AR land-falling latitude.

change in direction from WNW in September to WSW in December. ARs crossing Baja California were previously noted for their significant impacts on the precipitation climatology of the interior Southwestern U.S. [*Rutz and Steenburgh*, 2012; *Rivera et al*., 2014].

To further assess linkages of ARs to precipitation, especially heavy precipitation, we studied frequency and intensity of precipitation occurring during AR landfalls and on the subsequent day in the regions influenced by ARs. The process by which we identified AR-related precipitation in the 6 × 6 km gridded daily precipitation record [*Livneh et al*., 2013], as described in the supporting information section S2b, involves accumulating daily precipitation over days associated with AR landfalls over the region under the AR footprint (IVT $>$ 250 kg/m/s) interpolated from the coarse R1 grid to the fine *Livneh et al.* [2013] grid via *Shepard*'s [1968] method.

The impact of AR activity on seasonal precipitation is strongest during the extended winter season (OND and JFM), when almost all of AR days identified in the SIO-R1 catalog for the season are associated with rainy days (days with precipitation, Figure S8). ARs account for up to 65% of local seasonal precipitation at the coast and about 30% inland (Arizona, Nevada, and Idaho, Figures 2c and 2d). These wet season values are reflected annually (Figure 2a). Daily precipitation intensity expected on AR days reaches 200–300% of the local average daily precipitation intensity seasonally (Figure S9, OND, JFM) at the coastal ranges and the Sierra Nevada, as well as farther east into the Rockies. Spring and early summer account for the seasonally least frequent AR activity associated with the lowest seasonal precipitation contribution (Figure 2e). However, this contribution is still sizeable, as, particularly in late summer (Figure 2b), ARs bring to the North American west coast very infrequent but high-intensity precipitation (Figure S9a).

4. Climate-Scale Variability

Seeking to diagnose potentially predictable seasonal patterns of land-falling AR activity, we assess relationships between Pacific sea surface temperature (SST) patterns on the one hand and AR seasonal activity on the other. We use the updated NOAA Extended Reconstructed SST data, version 4 [*Huang et al*., 2015]. Past

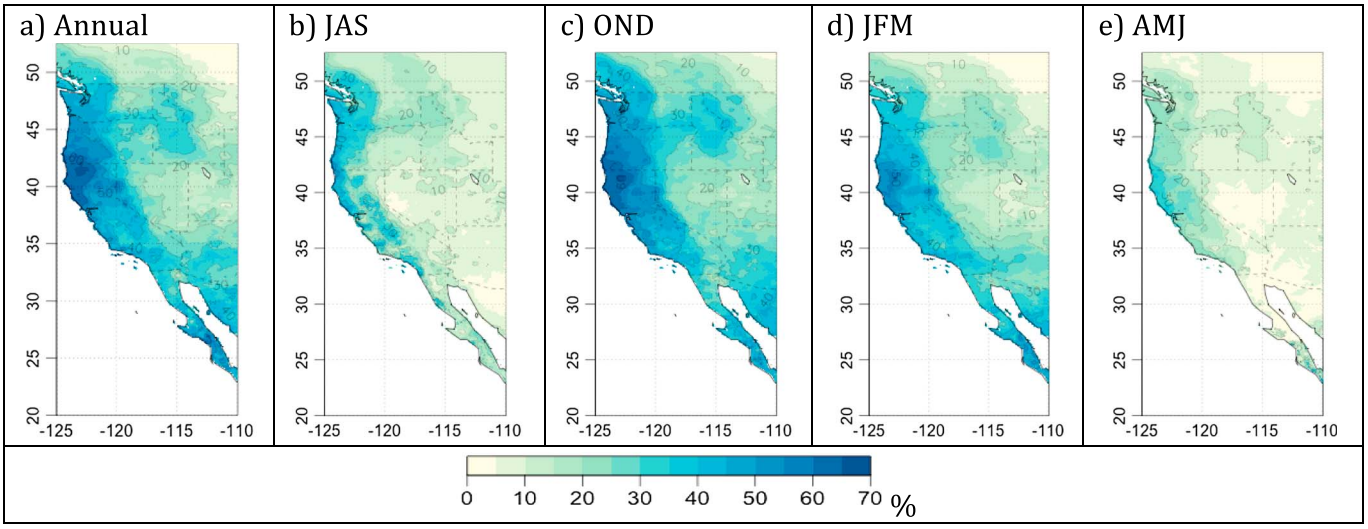

Figure 2. Contribution (%) of AR-related precipitation to (a) total annual and (b–e) seasonal precipitation. The gridded precipitation product is in situ observed daily precipitation interpolated onto a 6 × 6 km grid [*Livneh et al.*, 2013] and spanning 1950–2013.

work has linked seasonal variability and predictability in the frequency of heavy precipitation to SST patterns, particularly those associated with El Niño–Southern Oscillation (ENSO) and the Pacific Decadal Oscillation (PDO). *Gershunov and Cayan* [2003] examined predictive linkages between Pacific SST and conterminous U.S. heavy precipitation using canonical correlation analysis (CCA), which, in its diagnostic application, identifies temporally coupled patterns in two fields of variables and can also be used prognostically. Land-falling ARs, moving moisture evaporated from the ocean surface and being associated with heavy albeit mainly orographic precipitation in mountainous western North America, can a priori be expected to respond to Pacific SST forcing. We here apply CCA diagnostically to examine the validity of this expectation.

Although other seasons display meaningful connections between Pacific SST and North American precipitation, in our example we will focus on the late winter season (January–March, JFM), which has been previously identified as the season with the most predictable heavy precipitation [*Gershunov and Cayan*, 2003]. The version of CCA used here is "directional," i.e., sensitive to the fact that IVT is a vector field. *García-Bustamante et al.* [2012] have previously performed CCA on wind vectors. In performing directional CCA, we resolve both the *u* and *v* components of IVT, coupling IVT vectors at the land-falling R1 grids with SST over the tropical and north Pacific. We chose the broad SST domain covering the tropical and north Pacific to capture the important signals with known teleconnections to North America. The coastal IVT domain is salient for capturing the onshore vapor transport and therefore the AR intensity at landfall; however, for ease of interpretation, the result is displayed over the same IVT domain over which ARDT was applied. The western North American domain over which these results are related to precipitation represents the sink of AR-transported water vapor as it responds to teleconnected oceanic forcing via land-falling ARs. In the following analysis, IVT from R1, independent SST data, and gridded precipitation observations, all show consistent signals, thus bolstering our confidence in the results.

Figure 3 shows the three leading coupled modes derived from CCA applied to JFM SST and AR-IVT with implications for AR-related precipitation, while Figure S10 shows results of a similar analysis applied to SST and *total* seasonal IVT. Specifically, Figures 3a–3c display the leading mode of optimally correlated pairs of IVT and SST time series (Figure 3a) and the temporally coupled spatial patterns in SST and IVT (Figures 3b and 3c, respectively). The spatial patterns are displayed as correlations of the corresponding canonical correlates ($CC1_{IVT}$ or $CC1_{SST}$) with total IVT magnitude (colors) as well as with IVT vectors (vectors at coastal grid cells). Although only coastal IVT was used to summarize land-falling IVT activity, correlation patterns are shown with IVT magnitude over the entire IVT domain. We further correlated the temporal evolution of the IVT pattern associated with this leading coupled IVT-SST mode (Figure 3a, blue bars) with JFM AR-related precipitation (Figure 3d).

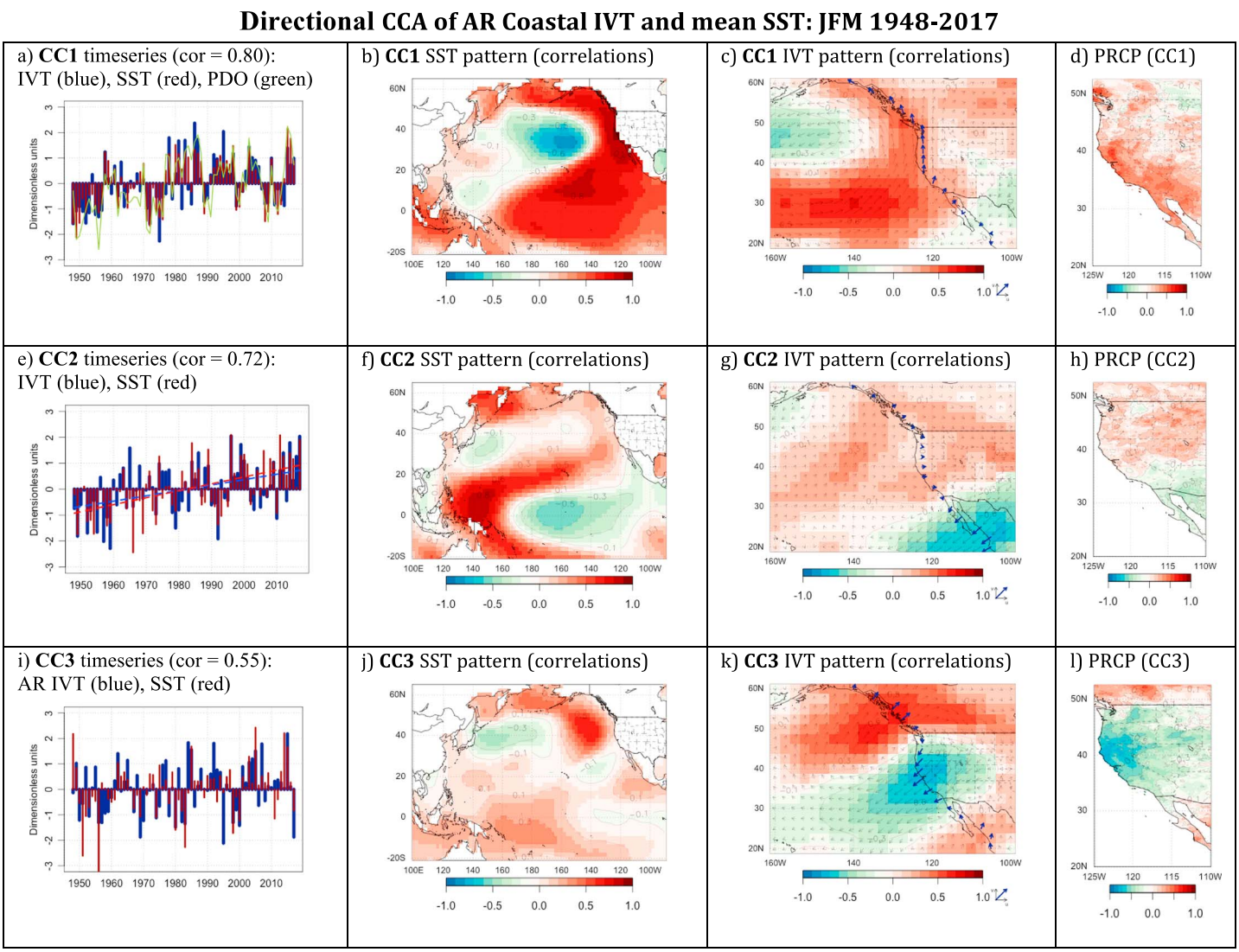

Figure 3. (a) Leading canonical correlates (time series) and their associated spatial patterns expressed as correlations between the time series and their respective fields of variables: (b) SST during the January–March, JFM, season and (c) seasonally summed AR-associated IVT. (d) Correlations between the IVT time series (Figure 3a, blue bars) and AR-associated precipitation. (e–h) The second leading coupled mode. (i–l) The third leading mode. The analysis was done on AR-related vector IVT confined to the coastal zone grid cells and expressed as correlations with the entire domain of AR-related IVT, both *u* and *v* components (arrows) and magnitude (colors), while the coastal grids that comprised the analysis domain are marked with thick arrows (Figures 3c, 3g, and 3k). Maximum possible arrow length is square root (2), shown to the right of the color scale, corresponding to unit ($r = 1$) *u* and *v* components. AR-associated JFM precipitation (PRCP) correlated with the corresponding modal IVT time series shown in Figures 3d, 3h, and 3l. Note that PRCP data span a shorter period (1950–2013) compared to SST and IVT data (1948–2017). The green curve in Figure 3a represents the time evolution of the JFM PDO (http://research.jisao.washington.edu/pdo/PDO.latest.txt), which is correlated with CC1SST at $r = 0.86$. The least squares-fitted trends in Figure 3e are significant with p values < 0.0005.

The leading CCA mode represents the impact of PDO [*Mantua et al.*, 1997] on land-falling AR activity. PDO (green line in Figure 3a) is correlated at ($r = 0.86$) with $CC1_{SST}$ and represents generally enhanced/diminished AR activity along the west coast of North America during positive/negative PDO phases. Moreover, directional CCA implies that the enhanced land-falling AR activity is associated with stronger southerly IVT along much of the coastline during positive PDO phases, although also weaker/stronger westerly IVT over British Columbia/extreme Southern California. This results in enhanced/diminished precipitation along the Sierra Nevada, the mountains of Southern California, and the extreme Southwestern Deserts (Figure 3d). Precipitation along the NNE-SSW oriented Cascades does not register this PDO signal associated with mostly meridional AR-IVT variability in that region. The coastal ranges of British Columbia, however, may derive more rainfall from enhanced southerly upslope IVT in land-falling ARs associated with the positive

phase of the PDO (Figures 3c and 3d). We note that the *seasonal total IVT variant* of this analysis (Figure S10, top row) shows a decidedly ENSO-related leading mode signal.

A long-term increasing trend in AR land-falling IVT is evident in the second CCA mode (Figure 3e), and this trend is related to the warming of the far western tropical Pacific (Figure 3f), which has been previously identified [*Wang et al*., 2015]. This trend explains little of IVT variance ($0.2 < r < 0.3$ amounting to less than 10% total AR-related IVT variability) but is associated with a broad enhancement of westerly IVT along the west coast of the U.S. and Canada, and a decline along the Mexican west coast (Figure 3g). The associated precipitation pattern shows broad gradual enhancement of AR-related precipitation over much of the interior Western U.S. and Southwestern Canada, but a decline in the Southwestern U.S. and northwestern Mexico (Figure 3h). The associated *total seasonal IVT result* (Figure S10, middle row) shows a clearer increasing IVT trend associated with broad warming of the Pacific Ocean (Figure S10f) and a related increase of Northwestern U.S. precipitation (Figure S10h). The directional nature of this result suggests that there may be a regional dynamical component to this observed trend, with which precipitation has consistently been keeping pace.

The third CCA mode (Figures 3i–3l) represents the sensitivity of land-falling AR activity on the "blob" of warm SST stretching southward from the Gulf of Alaska and off the Pacific Northwest (Figure 3j) which is consistent with a blocking high over the U.S. west coast [*Bond et al*., 2015]. The corresponding pattern in the AR-related IVT field (Figure 3k) involves strongly depressed onshore IVT at the US west coast, particularly in Northern California and much enhanced AR activity over southwestern Canada. AR-related precipitation associated with this mode is particularly diminished over Northern California (Figure 3l). These patterns are associated with the positive phase of the coupling, while the opposite patterns, i.e., cold "blob" in the northeastern Pacific, anomalously strong AR activity in Northern California and weak in southwestern Canada, are associated with the negative phase. This mode of coupled variability in SST and IVT patterns covaries with ~30% shared variability ($r = 0.55$), varies strongly on interannual time scales (Figure 3i), and was expressed particularly positively and strongly during the JFMs 2014–2015 California and Oregon drought. The *total seasonal IVT version* of this analysis (Figure S10, bottom row) involves enhanced onshore IVT at the U.S. West Coast, again particularly expressed at Northern California latitudes, associated with an anomalously warm Kuroshio Extension region and the strongest associated enhancement of precipitation in a broad swath from coastal Northern California and Oregon extending well into the interior Northwestern U.S. This mode appears to have contributed marginally to the most recent and anomalously wet winter in the western U.S., i.e., JFM 2017 (Figure S10i). The winter 2017 was notable for sporting the second strongest total IVT impinging upon the California coast in our 70 winter record (close second after JFM 1983, Figure S11a) and the strongest by far AR-related IVT (3 standard deviations above the mean, Figure S11b), which was undoubtedly instrumental in organizing the decisive lapse for the drought plaguing California in the early 21st century.

5. Summary and Conclusions

We have developed a new automated detection scheme for atmospheric rivers and applied it to 6 hourly IVT and IWV data in R1 to create a catalog of ARs land-falling upon the North American west coast—the SIO-R1 Catalog—which currently includes 69 full years (1948–2016) plus the winter of 2017. We have validated SIO-R1 against an established shorter and less extensive catalog (RNW) based on satellite-retrieved IWV data and independent finely resolved daily precipitation record [*Livneh et al*., 2013]. The SIO-R1 catalog yielded stronger seasonality of AR landfalls that are clearly associated with heavy precipitation over the coastal ranges and to some extent over the inland topography of the mountainous West.

Our AR detection methodology can be applied to any west coastal region of the globe in any reanalysis product or global climate model (GCM). In fact, it was recently applied to the NOAA 20th Century Reanalysis, which was used to successfully validate the SIO-R1 with respect to possible discontinuities associated with the start of the satellite era; no broadly systematic discontinuities in the SIO-R1 were detected. We plan to create additional catalogs of AR activity affecting the west coast of North America and elsewhere based on (a) finer-scale reanalyses to better resolve inland penetration of ARs [e.g., *Rutz et al*., 2014] and (b) GCM historical simulations and climate change projections—for examination of ARs' role in historical floods as well as past and future trends in AR activity associated with robust expectations of enhanced IVT

in a warmer world [*Lavers et al*., 2015] and projected stronger precipitation extremes along the west coast of North America [*Polade et al*., 2014], notably in California.

The SIO-R1 record of AR activity examined here provides a perspective on the seasonal cycle and interannual-interdecadal variability of AR activity affecting the hydroclimate of the North American West. We clearly detect the seasonal migration of peak AR activity from the Gulf of Alaska in the late summer-early fall, when AR landfalls are most frequent, to northern California in late fall-early winter. Climatological AR intensity does not closely follow AR frequency; intensity peaks in December in far Northern California where ARs are the prominent cause of flooding [*Ralph et al*., 2006]. We also see infrequent yet sustained AR landfalls over Baja California and Southern California State that appear to be largely IVT/wind driven in winter and IWV/moisture driven (with apparent tropical storm-related moisture origins) in late summer with a distinctive lull during the May and June peak of coastal low cloudiness in that region [*Clemesha et al*., 2016].

We have also examined the updated 70 winter (JFM) record for links between AR-related (as well as the seasonal total) IVT at the North American west coast and Pacific climate variability expressed in sea surface temperatures. Leading patterns that emerged indicate that land-falling AR activity is sensitive to modes of climate variability expressed in SST. These modes include most notably the PDO and associated eastern Pacific SST. They also include the northeastern Pacific warm "blob," described by *Bond et al.* [2015], suggesting a consistent role for ARs in the recent California drought. ARs also played a decisive role in this drought's demise via vigorous activity along the California coast, unprecedented on our 70 winter record.

Moreover, a long-term trend expressed broadly in stronger winter AR activity over the U.S. and Canadian west coast (weaker over Mexico) is associated with long-term warming of the western tropical Pacific; the latter SST trend has previously been identified in multiple observational data sets and explained by anthropogenic forcing [*Wang et al*., 2015]. Long-term precipitation changes over western North America have been very consistent with this trend. This broad increase in AR activity is corroborated by total seasonal IVT version of the analysis, where it is clearly associated with basin-scale ocean surface warming, as well as by a consistent increasing trend pattern in observed precipitation. These results suggest that the increase in IVT projected for the midlatitudes in response to global warming [*Lavers et al*., 2015] has been ongoing over at least the north Pacific, which calls for an investigation of the role of ARs in the projected enhancement of extreme precipitation over California and the Western U.S. [*Polade et al*., 2014] as well as a fresh investigation into observed changes already under way.

Interestingly, although ENSO is the main influence on *total* seasonal west coastal IVT, we did not detect clear and significant ENSO signals in land-falling AR activity. The SST-IVT linkages presented here display notable similarities and differences depending on whether CCA is applied to AR-related or total seasonal JFM IVT. The predictive capacity of such SST-IVT-precipitation linkages can and will be explored in a future article.

Besides uncovering modes of variability possibly accounting for seasonal and longer-term predictability, our CCA results demonstrate the reality of the highlighted modes of climatic variability reflected in at least three independent data sets ranging from reanalyzed AR activity to observed SST and precipitation, providing additional validation and confidence to the new SIO-R1 catalog.

Acknowledgments

This work was funded by Department of the Interior via the Bureau of Reclamation (USBR-R15AC00003, *Seasonal and extended-range predictability of atmospheric rivers and their associated precipitation*) and by the California Department of Water Resources (4600010378 UCOP2-11, *Development of Seasonal Outlooks for Atmospheric Rivers*). We also appreciate support from Climate Education Partners, a National Science Foundation funded project DUE-1239797. This study also contributes to DOI's Southwest Climate Science Center activities and NOAA's California and Nevada Applications Program award NA11OAR43101. We thank two anonymous reviewers for their constructive comments that led to an improved manuscript. The SIO-R1 can be accessed at http://cw3e.ucsd.edu/Publications/SIO-R1-Catalog/.

References

Bond, N. A., M. F. Cronin, H. Freeland, and N. Mantua (2015), Causes and impacts of the 2014 warm anomaly in the NE Pacific, *Geophys. Res. Lett.*, *42*, 3414–3420, doi:10.1002/2015GL063306.

Brands, S., J.M. Gutiérrez, and D. San-Martín (2016), Twentieth-century atmospheric river activity along the west coasts of Europe and North America: Algorithm formulation, reanalysis uncertainty and links to atmospheric circulation patterns, *Clim. Dyn.*, doi:10.1007/s00382-016-3095-6.

Clemesha, R. E., A. Gershunov, S. F. Iacobellis, D. R. Cayan, and A. P. Williams (2016), The northward march of summer low cloudiness along the California coast, *Geophys. Res. Lett.*, *43*, 1287–1295, doi:10.1002/2015GL067081.

Compo, G. P., et al. (2011), The twentieth century reanalysis project, *Q. J. R. Meteorol. Soc.*, *137*, 1–28, doi:10.1002/QJ.776.

Dettinger, M. D., F. M. Ralph, T. Das, P. J. Neiman, and D. R. Cayan (2011), Atmospheric rivers, floods and the water resources of California. *Water*, *3*, 445–478.

Dettinger, M. (2015), Sturm und Drang—California's remarkable storm-drought connection, *Hydrolink*, *1*, 21–22.

Eiras-Barca, J., S. Brands, and G. Miguez-Macho (2016), Seasonal variations in North Atlantic atmospheric river activity and associations with anomalous precipitation over the Iberian Atlantic Margin, *J. Geophys. Res. Atmos.*, *121*, 931–948, doi:10.1002/2015JD023379.

García-Bustamante, E., et al. (2012), North Atlantic atmospheric circulation and surface wind in the Northeast of the Iberian Peninsula: Uncertainty and long-term atmospheric variability, *Clim. Dyn.*, *38*, 141–160, doi:10.1007/s00382-010-0969-x.

Gershunov, A., and T. Barnett (1998), Inter-decadal modulation of ENSO teleconnections, *Bull. Am. Meteorol. Soc.*, *79*, 2715–2725.

Gershunov, A., and D. Cayan (2003), Heavy daily precipitation frequency over the contiguous United States: Sources of climatic variability and seasonal predictability, *J. Clim.*, *16*, 2752–2765.
Gorodetskaya, I. V., M. Tsukernik, K. Claes, M. F. Ralph, W. D. Neff, and N. P. M. Van Lipzig (2014), The role of atmospheric rivers in anomalous snow accumulation in East Antarctica, *Geophys. Res. Lett.*, *41*, 6199–6206, doi:10.1002/2014GL060881.
Guan B., and D. E. Waliser (2015), Detection of atmospheric rivers: Evaluation and application of an algorithm for global studies, *J. Geophys. Res. Atmos.*, *120*, 12,514–12,535, doi:10.1002/2015JD024257.
Huang, B., et al. (2015), Extended Reconstructed Sea Surface Temperature version 4 (ERSST.v4). Part I: Upgrades and intercomparison, *J. Clim.*, *28*, 911–930.
Jackson, D. L., M. Hughes, and G. Wick (2016), Evaluation of landfalling atmospheric rivers along the U.S. West Coast in reanalysis data sets, *J. Geophys. Res. Atmos.*, *121*, 2705–2718, doi:10.1002/2015JD024412.
Kalnay, E., et al. (1996), The NCEP/NCAR 40-year reanalysis project, *Bull. Am. Meteorol. Soc.*, *77*, 437–470.
Lavers, D. A., G. Villarini, R. P. Allan, E. F. Wood, and A. J. Wade (2012), The detection of atmospheric rivers in atmospheric reanalyses and their links to British winter floods and the large-scale climatic circulation, *J. Geophys. Res.*, *117*, D20106, doi:10.1029/2012JD018027.
Lavers, D. A., F. M. Ralph, D. E. Waliser, A. Gershunov, and M. D. Dettinger (2015), Climate change intensification of horizontal water vapor transport in CMIP5, *Geophys. Res. Lett.*, *42*, 5617–5625, doi:10.1002/2015GL064672.
Livneh B., E. A. Rosenberg, C. Lin, B. Nijssen, V. Mishra, K. M. Andreadis, E. P. Maurer, and D. P. Lettenmaier (2013), A long-term hydrologically based dataset of land surface fluxes and states for the conterminous United States: Update and extensions, *J. Clim.*, *26*, 9384–9392.
Mantua, N. J., S. R. Hare, U. Zhang, J. M. Wallace, and R. C. Francis (1997), A Pacific interdecadal climate oscillation with impacts on salmon production, *Bull. Am. Meteorol. Soc.*, *78*, 1069–1079.
Mundhenk, B. D., E. A. Barnes, and E. D. Maloney (2016), All-season climatology and variability of atmospheric river frequencies over the North Pacific, *J. Clim.*, *29*, 4885–4903.
Neiman, P. J., F. M. Ralph, G. A. Wick, J. D. Lundquist, and M. D. Dettinger (2008), Meteorological characteristics and overland precipitation impacts of atmospheric rivers affecting the west coast of North America based on eight years of SSM/I satellite observations, *J. Hydrometeorol.*, *9*, 22–47.
Payne, A., and G. Magnusdottir (2014), Dynamics of landfalling atmospheric rivers over the North Pacific in 30 years of MERRA reanalysis, *J. Clim.*, *27*, 7133–7150.
Polade, S. D., D. W. Pierce, D. R. Cayan, A. Gershunov, and M. D. Dettinger (2014), The key role of dry days in changing regional climate and precipitation regimes, *Nat. Sci. Rep.*, *4*, 4364, doi:10.1038/srep04364.
Ralph, F. M., and M. D. Dettinger (2011), Storms, floods, and the science of atmospheric rivers, *Eos Trans. AGU*, *92*, 265–266.
Ralph, F. M., P. J. Neiman, and G. A. Wick (2004), Satellite and CALJET aircraft observations of atmospheric rivers over the eastern North-Pacific Ocean during the El Niño winter of 1997/98, *Mon. Weather Rev.*, *132*, 1721–1745.
Ralph, F. M., P. J. Neiman, G. A. Wick, S. I. Gutman, M. D. Dettinger, D. R. Cayan, and A. B. White (2006), Flooding on California's Russian River: Role of atmospheric rivers, *Geophys. Res. Lett.*, *33*, L13801, doi:10.1029/2006GL026689.
Ralph, F. M., P. J. Neiman, G. N. Kiladis, K. Weickman, and D. W. Reynolds (2011), A multiscale observational case study of a Pacific atmospheric river exhibiting tropical-extratropical connections and a mesoscale frontal wave, *Mon. Weather Rev.*, *139*, 1169–1189, doi:10.1175/2010MWR3596.1.
Rivera, E. R., F. Dominguez, and C. L. Castro (2014), Atmospheric rivers and cool season extreme precipitation events in the Verde River Basin of Arizona, *J. Hydrometeorol.*, *15*, 813–829, doi:10.1175/JHM-D-12-0189.1.
Rutz, J. J., and W. J. Steenburgh (2012), Quantifying the role of atmospheric rivers in the interior western United States, *Atmos. Sci. Lett.*, *13*, 257–261, doi:10.1002/asl.392.
Rutz, J. J., W. J. Steenburgh, and F. M. Ralph (2014), Climatological characteristics of atmospheric rivers and their inland penetration over the Western United States, *Mon. Weather Rev.*, *142*, 905–921.
Shepard, D. (1968), A two-dimensional interpolation function for irregularly-spaced data, *ACM Natl. Conf.*, 517–524.
Swales, D., M. Alexander, and M. Hughes (2016), Examining moisture pathways and extreme precipitation in the U.S. Intermountain West using self-organizing maps, *Geophys. Res. Lett.*, *43*, 1727–1735, doi:10.1002/2015GL067478.
Wang, G., S. B. Power, and S. McGree (2015), Unambiguous warming of in the western tropical Pacific primarily caused by anthropogenic forcing, *Int. J. Climatol.*, *36*, 933–944.
Wick, G. A., P. J. Neiman, and F. M. Ralph (2013), Description and validation of an automated objective technique for identification and characterization of the integrated water vapor signature of atmospheric rivers, *IEEE Trans. Geosci. Remote Sens.*, *51*, 2166–76.
Zhu, Y., and R. Newell (1998), A proposed algorithm for moisture fluxes from atmospheric rivers, *Mon. Weather Rev.*, *126*, 725–735.